# Two-dimensional froths and the dynamics of biological tissues

B. Dubertret,* T. Aste,† H. M. Ohlenbusch,‡ and N. Rivier§
*Laboratoire de Dynamique des Fluides Complexes, Université Louis Pasteur, 3 rue de l'Université, Strasbourg 67084, France*
(Received 12 November 1997; revised manuscript received 26 May 1998)

Two-dimensional foams are used to model the evolution and the steady state of biological tissues. When only cell division occurs, we deduce the mode of division simply from the stationary distribution of the number of sides per cells, by inverting a system of coupled rate equations. Comparisons with experimental data confirm the method. We then discuss the time evolution of tissues evolving both through cell division and cell disappearance, theoretically and by topological simulations. Simulations reproduce realistically the steady state of the innermost layer of the human epidermis. We conclude that short-ranged topological information is sufficient to explain the evolution and stability of biological tissues. [S1063-651X(98)08111-2]

PACS number(s): 87.10.+e, 87.22.−q

## I. INTRODUCTION

Random cellular structures form the basic frame of many natural or engineered materials [1]. Among the many materials that have already been studied, epithelial tissues (the human epidermis, the epithelium of the cucumber, or the cork epithelium) are most striking for their ability to remain in steady state despite the fact that cells constantly divide or die. Better than any other systems, they can recover any externally induced departure from equilibrium (injuries or external stress).

Unlike other types of tissues (in vertebrates: nerve, muscle, blood lymphoid, and connective tissues), epithelial tissues have a scant extra-cellular matrix and tightly bounded, polyhedral-shaped cells. They cover all the cavities and free surface of the body. They form barriers to the movement of water, solutes, and cells from one body compartment to another. A deeper understanding of the cellular dynamics and the organization mechanisms of epithelial tissues may yield new biological insights relevant for some skin diseases (psoriasis) or wound healing.

The mechanisms that allow an epithelial tissue to return to its sound state involve intricate biological processes which eventually result in the division or disappearance of a cell. These two biological events produce local topological transformations that summarize the topological fate of a cell. They are ultimately responsible for the dynamics of the tissue.

The precise signals that induce a cell to divide or to detach (as, for example, from the basal layer of the human epidermis) are a matter of concern for biologists. Broadly, the issue is whether the equilibrium state of a sound tissue is the result of communication between the cells (be it short or long ranged) or whether it can be explained solely by the local environment of a cell (such as its topological characteristics).

Topologically, a two-dimensional cellular tissue is a froth, partitioning the plane into irregular polygons. Every vertex is the equilibrium point of three edges under tension (the line tension of the interface between two cells). A vertex with higher incidence number is not mechanically stable; it splits into several stable vertices with coordination number 3. In a froth, all the possible cell configurations can be explored by mitosis and disappearance. Cell mitosis and disappearance are specific combinations of the local, elementary topological transformations: (i) Exchange of neighbors ($T1$); (ii) disappearance of a three-sided cell ($T2$) or its inverse ($T2^{-1}$). There is only one random variable associated with a cell, namely the number $s$ of its sides (or its topological charge $q=6-s$). It is shuffled by mitosis or disappearance, but its averaged value $\langle s\rangle=6$ is fixed throughout the evolution of the tissue by Euler's relation and minimal incidence number. Corrections of order $1/N$ are due to boundary conditions, where $N$ is the total number of cells. These corrections vanish identically if, as here, periodic boundary conditions are used. They are negligible for large tissues (thermodynamic limit $N\to\infty$).

In this paper, computer simulations of froths evolving with cell mitosis and (or) disappearance are performed. The cellular networks consist of more than $10^4$ (except when testing the influence of the size of the network) cells on a lattice with periodic boundary conditions. Starting from different initial systems, ordered or disordered, we study their evolution when cells divide and (or) disappear under specific topological rules. We show that the evolution of a biological tissue depends only on the rules chosen for its dynamics, not on its initial states.

For tissues, such as the epithelium of the cucumber, evolving with mitosis only, inversion of the coupled rate equations for cell population [2] shows that the kernel of division can be deduced from the shape of the steady-state distribution. This establishes a link between the steady-state distribution and the dynamics that generates it. This result is confirmed by computer simulations and is used to predict the mode of division in cucumber [3], cork, amnion [3], and cultured Madin-Darby Canine-Kidney (MDCK) epithelial cells [4]. The predictions are in qualitative agreement with the experimental data available.

*Electronic address: benoit@maxent.u-strasbg.fr
†Electronic address: tomaso@ldfc.u-strasbg.fr
‡Electronic address: helgo@maxent.u-strasbg.fr
§Electronic address: nick@ldfc.u-strasbg.fr

 

When both cell division and disappearance occur, as is the case in the human epidermis, the simulations confirm the theoretical results obtained in [5]. We analyze the evolution of various systems in terms of the way cells divide and disappear. The results indicate that the ability of a real tissue to recover its sound steady state is explained by shape-dependent information stored in its cells. No additional information is needed.

We describe the epithelial tissue as a topological froth and study the consequences. Physically, a topological froth and its evolution result from space-filling by cells, separated by interfaces which carry all or most of the elastic energy [6]. This is indeed the case in a two-dimensional soap froth, where an $n$-sided cell shrinks (or expands) at a rate proportional to $(6-n)$, the local, topological information stored in the cell (Von Neumann's law). Von Neumann's law is the generalization to the froth of Laplace's law for an isolated bubble (whereby the pressure difference inside and outside the bubble, driving its evolution, is proportional to the surface's tension and to its curvature). Indeed, it can be obtained simply as the resultant of three interfaces with equal tension pulling on any one of the $n$ vertices of the cell. The topological description is therefore a direct consequence of the physics of the froth.

## II. RATE EQUATIONS

In order to characterize statistically the cut of a biological tissue whose cells divide and disappear, we used a local mean-field model based on the topology of the cells. Each cell is associated to a polygon (topological cell) whose number of sides equals the number of first neighbors of the biological cell. The cut of the biological tissue is thus associated to a connectivity graph of cell edges and three-fold vertices. No geometry or physical attributes such as vertex positions, edge curvatures, cell areas, or internal pressures are taken into account. The population of the $N$ cells of such a cellular system is partitioned into subpopulations of $N_s$ $s$-sided cells $(3 \leqslant s)$. The topological transformations (division and disappearance) of cells may produce a mix of the subpopulations. For instance, the symmetric division of a six-sided cell produces two five-sided daughter cells and increases by one the number of sides of two neighbors of the dividing cell. Similarly, the disappearance of a cell comes along with a modification of the number of sides of some of its neighbors, thus mixing the cell subpopulations.

The steady state of each subpopulation has been studied in [5], using a system of rate equations. For clarity and completion, we recall that the variation of the subpopulation of $s$-sided cells is given by

$$\frac{dp_s}{dt} = \sum_{k \geqslant 3} p_k P_m(k) D_m(k) \left\{ -\delta_{ks} + \Gamma(k \to s) + \frac{2}{k} [M_{s-1}(k) - M_s(k)] - p_s \right\} + \sum_{k \geqslant 3} p_k P_d(k) D_d(k) \left( -\delta_{ks} - M_s(k) + \sum_{i=-1}^{s-3} M_{s-i}(k) a_i(k) + p_s \right). \tag{1}$$

$p_s = N_s/N$ is the probability that a cell belongs to the subpopulation of $s$-sided cells. Changes of $p_s$ are due to (i) division of an $s$ cell, (ii) formation of an $s$-sided daughter cell, (iii) affected neighbors that have $s$ sides or $(s-1)$ sides before division, (iv) disappearance of an $s$ cell, (v) affected neighbors that have $(s-i)$ sides $(-1 \leqslant i \leqslant s-3)$ before disappearance. In the steady state, $dp_s/dt = 0$.

The steady-state equations [5] depend on the following: (a) $P_m(k)D_m(k)$ and $P_d(k)D_d(k)$, the conditional probability that an existing $k$-sided cell divides or disappears per unit of time; (b) the division kernel $\frac{1}{2}\Gamma(k \to s)$, conditional probability that a $k$-sided dividing cell has an $s$-sided daughter; (c) $a_i(k)$, the conditional probability that a $k$-sided detaching cell gives $i$ sides $(-1 \leqslant i \leqslant k-4)$ to one of its neighbors; (d) the nearest-neighbor topological correlations $M_s(k) = p_s A_{ks}$, where $p_s A_{ks} p_k N^2$ is the total number of pairs of neighboring $s$- and $k$-sided cells.

This equation has two parts. The first part describes the division mechanism [(i)–(iii)] and the second describes cell disappearance [(iv) and (v)]. If we forbid cell disappearance, $P_d(k)D_d(k) = 0$, Eq. (1) becomes the rate equation of a system evolving with cell division (or fragmentation) only. This equation, first introduced in [2], has been further analyzed by Delannay *et al.* in [7]. They confirmed that the linear variation of $M_s(k)$ on $k$, predicted by maximum entropy arguments [8,6] for structures in statistical equilibrium, is a very good assumption for systems evolving with cell division only. In [9], $A_{sk}$ is shown to depend linearly on $k$ and $s$, if no constraints other than those imposed by filling the space at random are imposed. $A_{sk} = (s-6)\sigma(k-6) + s + k - 6$. Here, $\sigma \leqslant \frac{1}{6}$ is a structural parameter, which is negative in biological tissues.

The second part of Eq. (1) is obtained for $P_m(k)D_m(k) = 0$. It governs the evolution of a system whose cells are only allowed to detach. During mitosis, only two neighbors gain one side. But when a cell detaches, several neighbors (sometimes all) can gain or lose sides. This effect is governed by $a_i(k)$, which has been computed in a mean-field approximation in [5] through the recursion relations

$$a_{-1}(k) = [(k-3)a_{-1}(k-1) + 1]/k \quad \text{for } k \geqslant 4,$$
$$a_i(k) = [(k-3)a_i(k-1) + 2a_{i-1}(k-1)]/k \quad \text{for } k \geqslant i+4,\ i \geqslant 0 \tag{2}$$

and the initial condition $a_{-1}(3) = 1$. It is properly normalized: $\Sigma_i a_i(k) = 1$. By definition, $a_i(k) = 0$ for $i > k-4$, $k \geqslant 3$. The sum rule $\Sigma_i i a_i(k) = 1 - 6/k$ insures that when a cell disappears, it removes six edges from the system, so that $\langle s \rangle = 6$ is conserved.

TABLE I. Comparison of the analytical solutions given in [7] with the solutions obtained numerically. To obtain the last significant digit, $p_k$ is computed for $k \leqslant 500$.

| Structure | Method | $p_4$ | $p_6$ | $\mu_2$ | $\sigma$ |
|---|---|---|---|---|---|
| $S_1$ | Analytical [7] | 0.217 72 | 0.125 17 | 12.883 | |
| | Numerical | 0.217 716 | 0.125 174 | 12.877 | 0.1173 |
| $S_2$ | Analytical [7] | 0.196 36 | 0.133 58 | 8.166 | |
| | Numerical | 0.196 363 | 0.133 580 | 8.166 02 | −0.0577 |

Equation (1) describes thus the interplay of two opposite phenomena: the creation of cells by mitosis and the disappearance of cells by detachment or death. When mitosis dominates $[\Sigma_k p_k P_m(k) D_m(k) > \Sigma_k p_k P_d(k) D_d(k)]$, the number of cells in the system increases, whereas it decreases if detachment is preponderant. A steady number of cells is ensured when cells divide at the same rate on average as they detach.

Up to now, Eq. (1) has been studied in particular cases [2,7,5]. In the next section, we show that its first part can be solved numerically for almost any value of the parameters $P_m(k) D_m(k)$ and $\Gamma(k \rightarrow s)$. The properties of the steady-state distribution $p_s$ (especially $p_6$ and the third moment $\mu_3$) classify cellular networks through their division kernel. Solutions of the whole equation are then obtained from topological simulations.

In general, the solution of Eq. (1) is the distribution $p_s$, characterized by its moments, specifically $\mu_n = \langle (s - \langle s \rangle)^n \rangle$, with $\langle s^n \rangle = \Sigma_s p_s s^n$ and $\langle s \rangle = 6$. The parameters are three sets, the division kernel $\Gamma(k \rightarrow s)$, $P_m(k) D_m(k)$, $P_d(k) D_d(k)$, and the structural parameter $\sigma$.

## III. STEADY-STATE SOLUTIONS UNDER DIVISION ONLY

The steady state of a cellular structure evolving with division only depends only on two sets of parameters, $P_m(k) D_m(k)$ and $\Gamma(k \rightarrow s)$, which define completely how cells divide. For given values of these parameters, we have solved numerically the first part of Eq. (1) using the module HYBRD from the package MINPACK (retrieved from NETLIB). This code finds a zero of a system of $n$ nonlinear functions [here, the first part of Eq. (1)] in $n$ variables (here $p_s$) by a modification of the Powell hybrid method. This code was found to be very robust for the problem we tackled. However, to avoid as much as possible numerical errors (unphysical distributions), we checked for each solution obtained that $0 \leqslant p_s \leqslant 1$, $\Sigma_s p_s = 1$, and $\Sigma_s s p_s = 6$. All the solutions presented here satisfy these two conditions within $10^{-10}$ and are zeros of the first part of Eq. (1) with an error smaller than $10^{-15}$.

Furthermore, to test the reliability and the precision of the method, we compared the numerical solutions with the analytical ones, in the two cases where analytical solutions exist [7], namely for a flat kernel $\Gamma(k \rightarrow s) = 2/(k-1)$ $(3 \leqslant s \leqslant k+1)$, when dividing cells are selected randomly among $N$ cells $[P_m(k) D_m(k) = 1/N$, case $S_1]$ and when dividing cells are randomly selected by first choosing one edge at random $[P_m(k) D_m(k) = k/6N$, case $S_2]$. Table I illustrates the reliability of the numerical method.

Once the stability of the numerical method has been verified, we solved Eq. (1) for different values of the parameters $P_m(k)$ and $\Gamma(k \rightarrow s)$. To explore the widest possible range of steady-state solutions, we chose a one-parameter-dependent exponential function for $P_m(k) D_m(k) = C \exp(\alpha k)$ (where $C$ is a constant of normalization), $P_m(3) = P_m(4) = 0$, and five division kernels with different levels of symmetry (given in the Appendix). We chose an exponential functional form for the rate of division for two reasons. (i) From the data given by Lewis for the cucumber one can deduce that $P_m(k) D_m(k) = C \exp(1.4k)$ [2]. We supposed that other biological tissues had similar rates. (ii) This functional form is very convenient to explore the effect of a (strongly) increasing or decreasing rate on the steady-state distribution.

For each kernel, we solved numerically the first part of Eq. (1). The parameter $\alpha$ can range from $-4$ to 4, but it must be constrained so that every solution respects $\Sigma_s p_s = 1$ and $\Sigma_s s p_s = 6$ with the requirements defined above. Each set of parameters yields a steady-state solution of a cellular system evolving with cellular division.

The numerical solutions, as a function of the parameters, can be classified into different families. Two solutions are members of the same family if they have the same division kernel.

Consider a given family. Two different members of the family are characterized by different $P_m(k) D_m(k)$, i.e., by the way dividing cells are chosen. When $P_m(k) D_m(k)$ is an increasing function of $k$, many-sided cells divide preferentially and the associated distributions $p_s$ are narrow (small $\mu_2$), with large $p_6$ $(\approx \frac{1}{2})$. By contrast, decreasing functions $P_m(k) D_m(k)$ yield very broad distributions, associated with large $\mu_2$ and low $p_6$. A constant $P_m(k) = 1/N$ corresponds to a random choice of the cells and is associated with broad distributions (cf. solution $S_1$).

We illustrate this behavior in Figs. 1 and 2 for the family defined by a fully symmetric kernel.

Figures 1 and 2 indicates that the stationary distributions within the same family are usefully characterized by $p_6$ and the second moment $\mu_2$ or the third moment $\mu_3 = \Sigma_s (s - \langle s \rangle)^3 p_s$. As usual, $\langle s \rangle = 6$ is fixed. Both $\mu_2$ and $\mu_3$ are decreasing monotonically with increasing $p_6$, or with increasing $\alpha$, the parameter of the rate of division $P_m(k) D_m(k) = C \exp(\alpha k)$. Accordingly, $p_6$ decreases monotonically with decreasing $\alpha$. This is not the case for $p_5$ and $p_7$.

It has been inferred by the maximum entropy argument that the relation between $\mu_2$ and $p_6$ is universal in two-dimensional froths in statistical equilibrium for $p_6 > 0.33$ [10]. This universality had been suggested empirically earlier [11]. Thus, different distributions with the same $p_6 > 0.33$

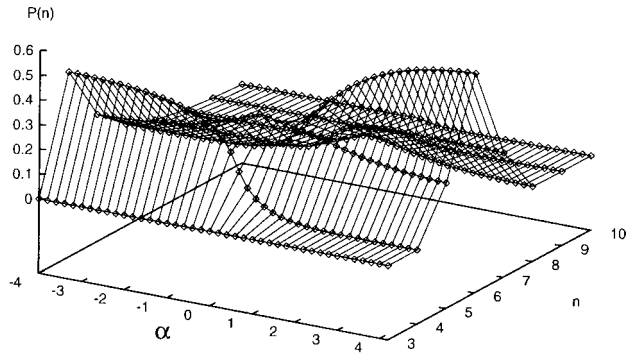


FIG. 1. Division only. The distribution $p_n$ is the solution of the first part of Eq. (1) for a fully symmetric division kernel and $P_m(k)D_m(k)=C\exp(\alpha k)$ for $-4\leqslant\alpha\leqslant 4$. For low values of $\alpha$, the distribution is very broad ($\mu_2>30$), but becomes very narrow as $\alpha$ approaches 4 ($\mu_2<\frac{1}{2}$). $\mu_2$ increases and $p_6$ decreases monotonically as $\alpha$ decreases. By contrast, $p_5$ and $p_7$ are not monotonic in $\alpha$.

have the same second moment. As Fig. 3 illustrates, they are distinguished by the third moment $\mu_3$, which measures the asymmetry of the distribution about $\langle s\rangle=6$, together with its width. Thus, to distinguish between different families, stationary distributions should be characterized by $p_6$ and $\mu_3$.

Precisely, if the functional form of $P_m(k)D_m(k)$ is known, there is a one-to-one map between the two most relevant parameters of the stationary distribution $(p_6,\mu_3)$ and the parameters governing the dynamics of the cells: the division kernel and the rate of cell division. This classification is indicated in Fig. 3: for each family (each type of division kernel), there is a relation between $\mu_3$ and $p_6$, parametrized by $\alpha$, i.e., by the rate of division. Each curve of Fig. 3 represents this relation, for the five different families whose division kernel is given in the Appendix. The curves are nonintersecting. Figure 3 can be regarded as a map of the dynamics. To each point $(p_6,\mu_3)$ corresponds a division kernel and a value of $\alpha$ (i.e., the probability that a $k$-sided

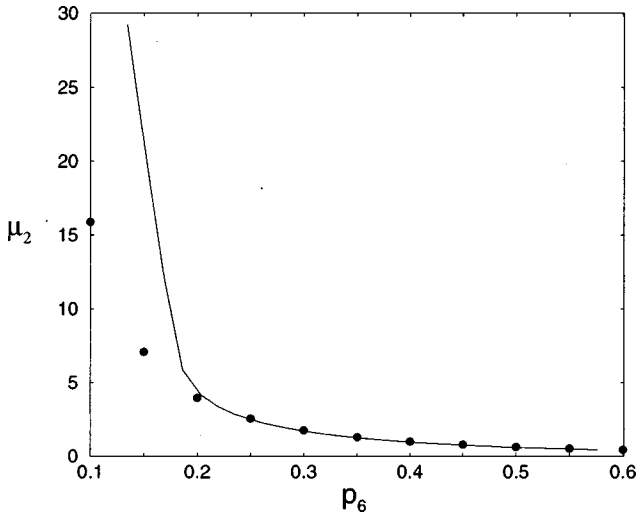


FIG. 2. Division only. Plot of the second moment of the distributions solution of the first part of Eq. (1) as a function of $p_6$, for a fully symmetric division kernel, and $P_m(k)D_m(k)=C\exp(\alpha k)$. Small $\mu_2$ are associated with large values of $\alpha$. $p_6$ decreases as $\alpha$ decreases (see Fig. 1). The full dots correspond to $\mu_2 p_6^2=1/2\pi$, inferred to be universal for $0.33<p_6<0.66$ [10].

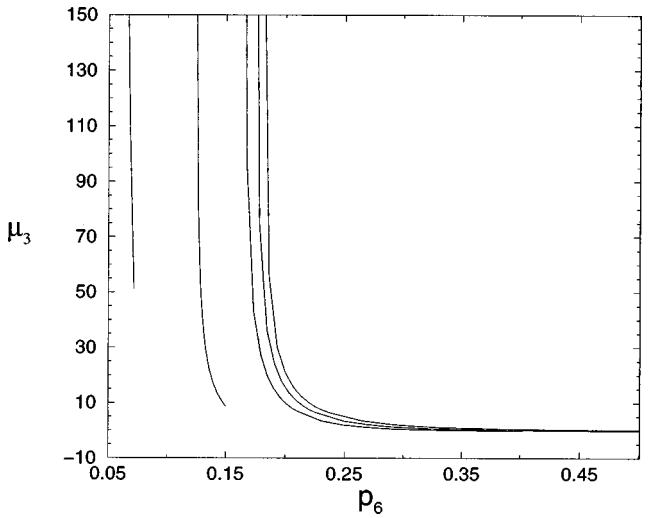


FIG. 3. Each curve is a representation ($\mu_3$ as a function of $p_6$) of the distributions solution of Eq. (1) (division only) when $\Gamma(k\rightarrow s)$ is fixed and $P_m(k)D_m(k)=C\exp(\alpha k)$, $\alpha\in[-4,4]$. Five different division kernels are represented (from left to right: $\Gamma_1$ to $\Gamma_5$, see the Appendix). The most asymmetric kernel ($\Gamma_1$) corresponds to the leftmost curve. As the kernel becomes more symmetric, its associated curve moves to the right. The rightmost curve corresponds to the fully symmetric kernel ($\Gamma_5$). This family-specific relation between $\mu_3$ and $p_6$ is to be contrasted with the relation between $\mu_2$ and $p_6$ (Fig. 2), which is the same for every family (i.e., independent of the division kernel).

cell divides). We have thus inverted the first part of the system of Eq. (1). From any distribution resulting from cell division only, we obtain the dynamics that drove the froth to its steady state. Other functional forms for the rate of division give qualitative results identical to the ones plotted in Fig. 3. The overall position and shape of the curves may change slightly. Comparison and prediction for real tissues are given in Sec. V.

## IV. SIMULATIONS

When $P_d(k)D_d(k)=0$, the numerical resolution of Eq. (1) is robust and easy. However, when the full equation is considered, the code used becomes much more unstable, and even if some solutions can be obtained [5], analysis similar to the one done in the previous sections is impossible. For most of the parameters we tried, the solver was not able to find a physical solution, with probabilities $0\leqslant p_k\leqslant 1$ and a mean number of sides per cell equal to 6. Topological simulations are not subject to the same drawbacks. The conditional probabilities that a $k$-cell divides or disappears are chosen arbitrarily, and the system is left to evolve.

A simulation starts with the generation of a hexagonal cellular network of $N$ cells with periodic boundary conditions (typically, $N=10^4$). The network can be taken as initial structure, or it can be disordered by performing $30N$ $T1$ transformations (exchange of neighbors) on edges chosen at random. If a $T1$ produces a two-sided cell or a cell sharing an edge with itself, it is refused. Throughout the simulation, the cellular network is purely topological, consisting of a connectivity graph of cell edges and threefold vertices. Only the graph is retained during the simulations; there are no geometric or physical attributes such as vertex positions,

TABLE II. The conditional probabilities per move of division, $P(m|k)$, of a $k$-sided cell, for different modes $a$, $b$, $c$, and $d$ of simulation.

| $k$ | 3 | 4 | 5 | 6 | 7 | 8 | 9 | 10 | >10 |
|---|---|---|---|---|---|---|---|---|---|
| $P(m\|k)^a$ | 1 | 1 | 1 | 0 | 0 | 0 | 0 | 0 | 0 |
| $P(m\|k)^b$ | 0 | 0 | 0 | 0 | 1 | 1 | 1 | 1 | 1 |
| $P(m\|k)^c$ | 0 | 0 | 0 | 0.01 | 0.02 | 0.05 | 0.1 | 0.2 | 1 |
| $P(m\|k)^d$ | 0 | 0 | 0.01 | 0.05 | 0.4 | 1 | 1 | 1 | 1 |

edge curvatures, cell areas, or internal pressures.

Two types of dynamics have been performed: cell division only and cell division together with cell disappearance. In both cases, the simulation consists of a series of successive moves numbered 0,1,2,3,.... A move is defined as follows.

A cell is chosen at random. It has $k$ neighbors, say. (i) In the case of division only, the cell is divided symmetrically with the probability $P(m|k)$ and left unchanged with the probability $1-P(m|k)$. (ii) In the case of division and disappearance, if the move number is even, the cell is divided symmetrically with the probability $P(m|k)$ and left unchanged with the probability $1-P(m|k)$. If the move number is odd, the cell is made to disappear with the probability $P(d|k)$ and left unchanged with the probability $1-P(d|k)$.

A move is unsuccessful if the cell chosen is left unchanged, successful otherwise. The disappearance of a $k$-sided cell is obtained with a succession of $(k-3)$ $T1$ performed on its edges chosen randomly, followed by a $T2$. If a $T1$ is not possible, as is the case when the edge chosen is also that of a three-sided neighbor, a $T2$ is performed instead. As a consequence, the disappearance of one cell may induce the disappearance of several cells.

In all simulations, unless specifically mentioned, cells divide with a symmetric kernel. The choice of the neighbors affected by the division is random, as is the choice of the daughter cell with the extra edge when $k$ is odd.

The only parameters of the simulations are the two distributions $P(m|k)$ and $P(d|k)$, which are unrelated. They are equivalent to the parameters $P_m(k)D_m(k)$ and $P_d(k)D_d(k)$, respectively, defined in Eq. (1). In the simulations, the time is measured by the total number of moves attempted (successful or not).

### A. Cellular division

We investigated the evolution of systems evolving with division only for four different choices ($a$,$b$,$c$,$d$) of $P(m|k)$, given in Table II.

In order to compare the results of the simulations with the solutions of the first part of Eq. (1) (Sec. II), $P(m|k)$ should have been taken as proportional to $\exp(\alpha k)$. If we do so, since $P(m|k)<1$ for all $k$, most $P(m|k)$ are close to 0, and the time needed to reach equilibrium in the simulations is prohibitive. This is why the compromise $P(m|k)=1$ for $k>k_0$ and has been chosen.

In mode $a$, only cells with a small number of sides ($k \leqslant 5$) divide, and we anticipate a very disordered steady state. By contrast, in mode b, only cells with a large number of sides ($k \geqslant 7$) divide. Modes $c$ and $d$ have been chosen to reproduce the distributions of natural structures.

We computed the integral rate of growth $R(t)$, defined as the ratio of the total number of divisions performed to the total number of divisions attempted:

$$R(t)=\frac{N(t)-N(0)}{t}. \tag{3}$$

The average increase of cells per move $dN(t)/dt = \Sigma_k p_k(t)P(m|k)$ is related to $R(t)$ through Eq. (3) by

$$\sum_k p_k(t)P(m|k)=\frac{dN(t)}{dt}=\frac{d[N(t)-N(0)]}{dt}=\frac{d}{dt}[tR(t)]. \tag{4}$$

In all modes, $R(t)$ reaches an asymptotic value $R_\infty$ (Fig. 4), independent of the time. This implies, through Eq. (4), that $\Sigma_k p_k(t)P(m|k)=R_\infty$, which strongly suggests, since $P(m|k)$ is independent of the time, that the distribution $p_k(t)$ is stationary. Thus, when $R(t)=R_\infty$, it is very likely that the system remains statistically unchanged, and that its second moment is constant as observed in Fig. 5.

Within a family, $R_\infty$ depends on the values of $P(m|k)$. In general, low values of $R_\infty$ are associated with the more ordered structures. We found that $R_\infty=0.73$, 0.19, 0.05, and 0.01 for systems $a-d$, respectively (Fig. 4).

Similarly, the number of moves necessary for $R(t)$ to reach its asymptotic value $R_\infty$ depends on $P(m|k)$. But it also depends on the size and the disorder of the initial system. For each mode $a-d$, we started the simulation from two disordered initial networks of 100 cells and $10^4$ cells, respectively. When small systems are considered, $R_\infty$ is reached after $2\times10^4$ divisions, that is, 200 times the size of the initial network. The evolution of large systems $[N(t=0)=10^4]$ indicates that $R(t)$ converges to its limit faster for systems with small $R_\infty$ (Fig. 4). System $d$ reached $R_\infty$ after only $7\times10^4$ divisions while system $a$ is still far from $R_\infty$ after $25\times10^4$ divisions. We expect the rate of systems $a$ and $b$ to reach its asymptotic value after $200\times10^4$ divisions, that is, 200 times the size of the initial network.

The steady state reached by a system evolving with division only is independent of the initial disorder of the froth. We have obtained statistically identical froths starting from the hexagonal lattice ($\mu_2=0$) or from a very disordered network with $\mu_2>13$ (Fig. 5). In the first case, the system evolves from order to disorder, whereas in the second case it is the opposite. Division is thus a local topological transformation, which, if performed with given rules, leads any cellular system into a steady distribution whatever its initial state.

Consider a system that is driven away from its steady state by some external disturbance (physical or biological). If

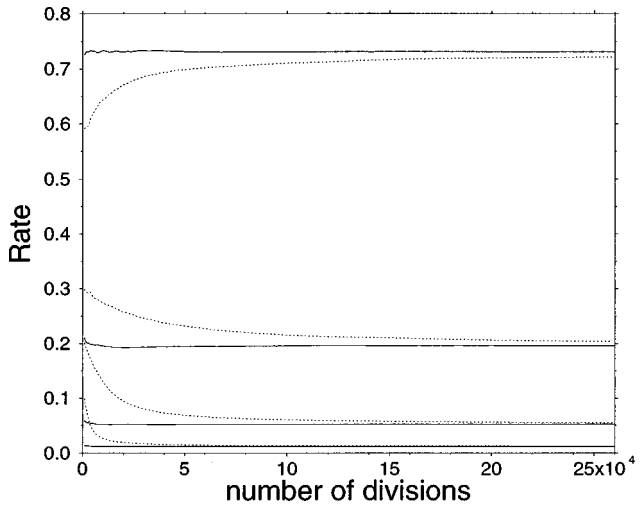


FIG. 4. Rates of division (ratio of number of divisions performed to the number of divisions attempted) for systems $a-d$, from top to bottom. Plain lines: initial disordered structure of 100 cells. Dotted lines: initial disordered structures of $10^4$ cells. We have plotted the rate of division as a function of the number of divisions instead of the time (number of moves) because only successful moves (divisions) make the system evolve towards stationarity. A stationary distribution is reached well before $R(t)=R_\infty$: Using $p_k(t)=p_k$ in Eq. (4), one obtains $R(t)=R_\infty+B/t$, where $B$ is a constant related to the initial size of the system and to $P(m|k)$. In terms of the number of divisions ($N_{\mathrm{div}}$), the distribution is stationary when $R(N_{\mathrm{div}})=R_\infty(1+1/[N_{\mathrm{div}}/B-1])$. Thus, the ($N_{\mathrm{div}}$) scale should be rescaled by $B$.

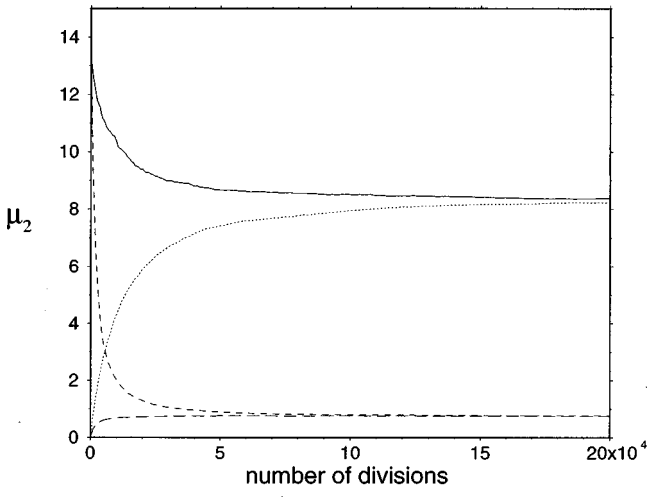


FIG. 5. Evolution of the second moment of two systems as divisions are performed. Initial structures have $10^4$ cells. If the initial network is a hexagonal lattice [raising curves, $\mu_2(t=0)=0$], the system evolves towards a disordered state. If the initial network is highly disordered [descending curves; $\mu_2(t=0)=13.2$], the system evolves towards a less disordered state. The final state (statistical equilibrium) of each mode of simulation is independent of the initial configuration of the network. The system associated to the two upper curves is the system $S_2$ of Sec. III. Cells, chosen by first selecting an edge at random, divide with a flat division kernel. The cells of the system associated to the two lower curves divide with mode $d$ (symmetric division: many-sided cells are more likely to divide than few-sided cells; cf. Table II).

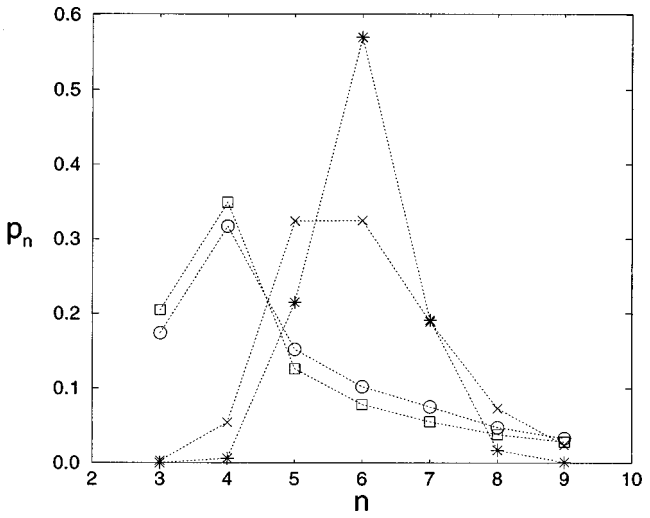


FIG. 6. Simulations with division and disappearance. Distributions of the number of sides for the modes ($e-h$). Circles: mode $e$; squares: mode $f$; crosses: mode $g$; and stars: mode $h$. The parameters defining each mode are given in Table III.

the information contained in the cells pertaining to the way they divide [i.e., $P(m|k)$ and $\Gamma(k\rightarrow s)$] is unchanged, the system will self-regulate to return to its original steady state.

### B. Division and detachment

We analyzed the disorder and the temporal evolution of four systems ($e$, $f$, $g$, and $h$) for which there is no systematic proliferation of cells or no catastrophic disappearance of all the cells over a long time. Typically, for all times between 0 and $t=N(0)^2$, $N(t)$ is bounded between $N(0)/5$ and $5N(0)$. The different choices of the parameters are given in Table III.

In modes $e$ and $f$, few-sided cells divide and many-sided cells detach, whereas in modes $g$ and $h$, many-sided cells divide and few-sided cells detach.

The distributions obtained in modes $e$ and $f$ have broad unimodal distributions centered at $k=4$ (Fig. 6) and high $\mu_2$ ($\mu_2^e>40$, $\mu_2^f\approx 21$). The distributions are stationary (within statistical fluctuations), with a large tail, which induce large fluctuations of $\mu_2$ (Fig. 7).

Conversely, distributions obtained with modes $g$ and $h$ have narrow unimodal distributions (Fig. 6) centered on 6, with small $\mu_2$ ($\mu_2^g=1.42$, $\mu_2^h=0.5$). Those systems are highly ordered and statistically similar to natural systems (see Sec. V). Their steady-state distributions fluctuate much less than those of systems $e$ and $f$ (Fig. 7).

For systems $e-h$, we computed $R^m(t)$ [$R^d(t)$], the integral rate of division (disappearance), defined as the ratio of the total number of division (disappearance) performed to the total number of division (disappearance) attempted. As in the case of division only, the two rates can be expressed in terms of $p_k(t)$:

$$R^m(t)=\sum_k p_k(t)P(m|k),$$

$$R^d(t)=\sum_k p_k(t)P(d|k).$$

TABLE III. The conditional probabilities per move of division, $P(m|k)$, and disappearance, $P(d|k)$, of a $k$-sided cell, for different modes $e$, $f$, $g$, and $h$ of simulation. Attempted divisions [with $P(d|k)=0$] and attempted disappearances [with $P(m|k)=0$] are alternated.

| $k$ | 3 | 4 | 5 | 6 | 7 | 8 | 9 | 10 | >10 |
|---|---|---|---|---|---|---|---|---|---|
| $P(m\|k)^e$ | 1 | 1 | 0 | 0 | 0 | 0 | 0 | 0 | 0 |
| $P(d\|k)^e$ | 0 | 0 | 0.305 | 1 | 1 | 1 | 1 | 1 | 1 |
| $P(m\|k)^f$ | 1 | 0.3 | 0.2 | 0.1 | 0 | 0 | 0 | 0 | 0 |
| $P(d\|k)^f$ | 0 | 0 | 0 | 0.09 | 0.295 | 0.7 | 1 | 1 | 1 |
| $P(m\|k)^g$ | 0 | 0 | 0.04 | 0.12 | 0.16 | 0.4 | 0.5 | 1 | 1 |
| $P(d\|k)^g$ | 1 | 0.8 | 0.2 | 0.05 | 0.011 | 0 | 0 | 0 | 0 |
| $P(m\|k)^h$ | 0.05 | 0 | 0 | 0 | 0.05 | 0.5 | 0.95 | 1 | 1 |
| $P(d\|k)^h$ | 1 | 0.515 | 0.069 | 0 | 0 | 0 | 0.069 | 0.515 | 1 |

For modes $e-h$, $R^m(t)$ and $R^d(t)$ reach an asymptotic value ($R^m_\infty$ and $R^d_\infty$, respectively), independent of the time (Fig. 8). This strongly suggests that the distribution becomes stationary, $p_k(t)=p_k$. For all these modes, $R^m(t)\geqslant R^d(t)$, even though the number of cells is not increasing overall. This is because the disappearance of a cell may induce the disappearance of some of its three-sided neighbors. However, modes $g$ and $h$ have a very narrow distribution with hardly any three-sided cells, and $R^m_\infty=R^d_\infty$ to a very good approximation.

The temporal evolution of systems $e-h$ is characterized by periods of cell gain alternating with periods of cell loss. This fluctuating behavior is found to have the same erratic characteristics, whatever time scale is considered (Fig. 9). At a given time of its evolution, a system can be simultaneously in a different trend according to the scale at which we look. For example, on a short-range and middle-range time scale, a system may lose cells even though it is growing over a long-range time scale of growth (star in Fig. 9). It is impossible to predict, within a given time scale, whether the system will eventually grow or die away.

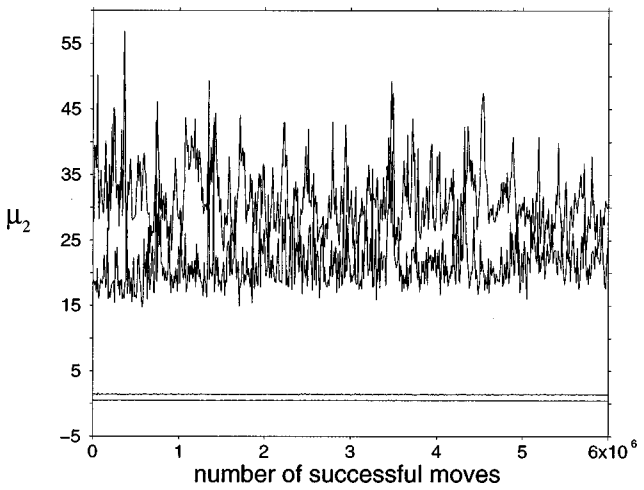


FIG. 7. Fluctuations of the second moment of modes $e-h$ (top to bottom) as divisions and disappearances are performed. The two highly disordered modes $e$ and $f$ evolve with large fluctuations of their second moment. By contrast, the second moment of the less disordered modes $g$ and $h$ is constant (within statistical fluctuations). All distributions are stationary, but divisions of cells with many sides induce huge fluctuations in $\mu_2$ in modes $e$ and $f$, where the distribution has a larger tail.

Long-range fluctuations of the number of cells introduce a variation of the size of the system by a factor of 5. Consequently, either the average surface of a cell or the area of the substrate should be flexible. Furthermore, as in the case of division only, the evolution of systems whose cells divide and disappear is fully determined by the topological rules given for division and disappearance. It is independent of the size or the disorder of the initial system.

## V. COMPARISON WITH NATURAL SYSTEMS

As mentioned in the Introduction, the dynamics of biological tissues formed from confluent cells can be modeled with 2D froths evolving with divisions and/or detachments. Some epithelial tissues evolve solely with cell division (epithelium of the cucumber), whereas the dynamics of more complex ones (mammalian epidermis) involve also cell disappearance. In this section, we use the technique developed in Sec. III to predict the way cells divide in natural systems and compare the results with the data available. We then use the simulations of Sec. IV to produce systems statistically equivalent to natural ones. We conclude that topological information limited to the cell suffices to mimic the evolution of a biological tissue.

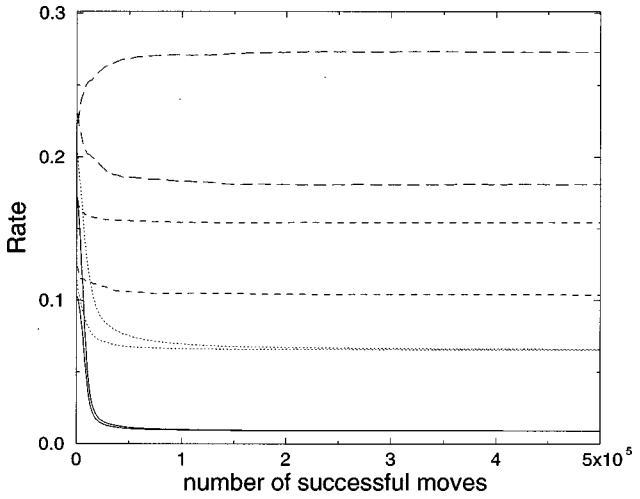


FIG. 8. Evolution of the rates of divisions (ratio of the number of divisions attempted to the number of divisions performed) and disappearance (ratio of the number of disappearances attempted to the number of disappearances performed) for modes $e$, long-dashed; $f$, dashed; $g$, dotted; and $h$, solid line. For all modes, $R^m_\infty\geqslant R^d_\infty$.

### A. Division only

We analyzed the distributions of four different biological tissues evolving with division only: the epithelium of a 100 mm cucumber [3] (i), the cork (ii), human amnion [3] (iii), and cultured MDCK [4] (iv).

We computed the third moment of each experimental distribution; their labels are given in brackets $(p_6,\mu_3)$. The cucumber (0.474,0.08) is characterized by a very narrow distribution $p_s$ centered on 6 and a small $\mu_3$. The cork (0.3784,0.179) has a wider distribution centered on 6 and a fairly high $\mu_3$, denoting an asymmetrical distribution. The human amnion (0.397,0.06) has the lowest $\mu_3$ and thus the most symmetrical distribution. As for the cultured MDCK (0.364,0.675), its steady-state distribution is centered on 6, very narrow and fairly asymmetric: $p_5=0.310$ and $p_7=0.184$.

We then reported each couple $(p_6,\mu_3)$ in Fig. 10, a magnification of Fig. 3, and deduced for each tissue the values of the parameters $P(m|k)$, and $\Gamma(k\rightarrow s)$, characterizing the way cells divide.

Although the distributions of (ii) and (iii) have different $(p_6,\mu_3)$, they are almost on the same curve $\mu_3=f(p_6)$ (Fig. 10). This suggests that they have very similar kernels of division. The cells of the cork and human amnion thus divide with the same type of symmetry. The two systems differ by the conditional probability that their cells divide. We found that $P_m^{ii}(k)D_m^{ii}(k)\approx\exp(1.1k)$ and $P_m^{iii}(k)D_m^{iii}(k)\approx\exp(1.35k)$. Thus, many-sided cells divide with a higher probability in the human amnion than in the cork.

The cucumber's cells belong to a different family. They divide more symmetrically with a conditional probability $P_m^{i}(k)D_m^{i}(k)\approx\exp(1.4k)$. These observations are in very good agreement with the data given by Lewis [3]. The family of the cultured MDCK is close to that of the cucumber, but with a division kernel that is almost fully symmetric, as observed experimentally. We found that $P_m^{iv}(k)D_m^{iv}(k)\approx\exp(0.9k)$

The values of the parameters of each system, approximated from Fig. 10, can be computed with more precision by solving directly the first part of Eq. (1). They can then be

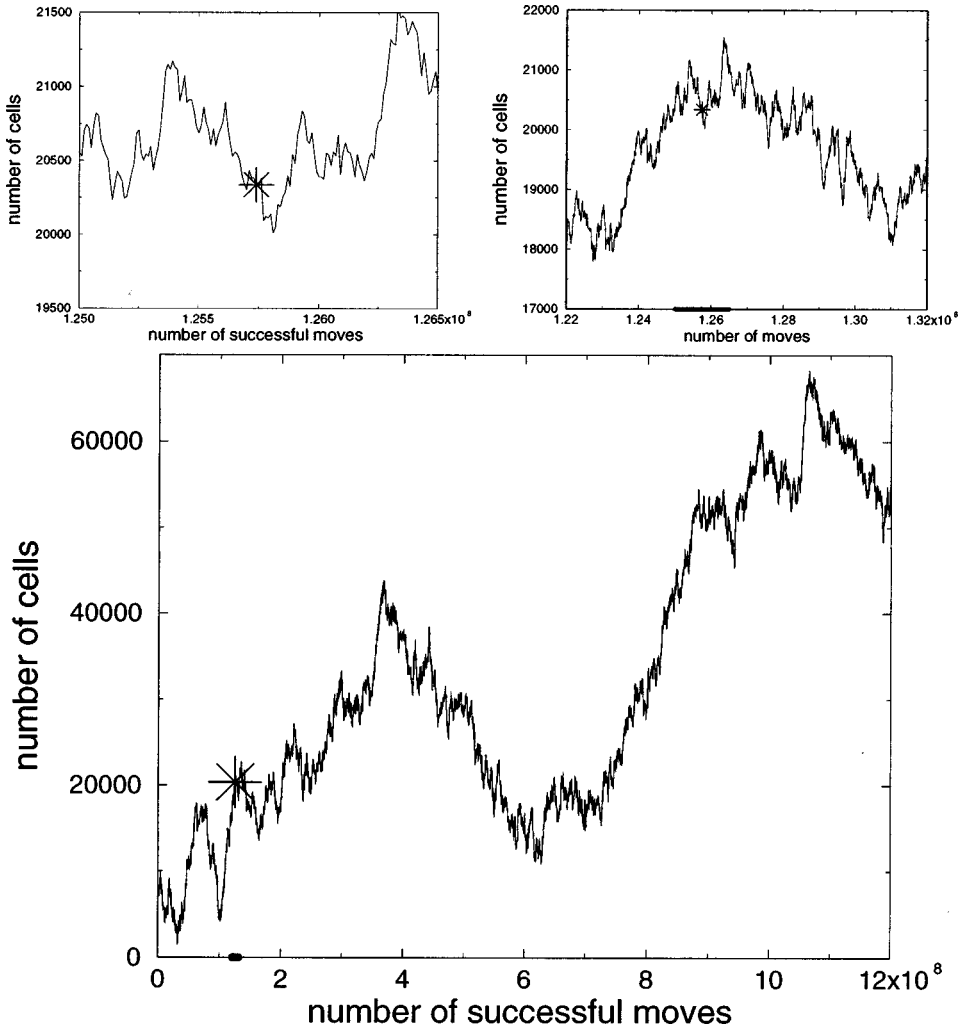


FIG. 9. Evolution of the system as divisions and detachments are performed (mode *h*). Three time scales are represented, increasing clockwise from top left. A star represents the number of cells (20 337) of the system after $12\,574\times10^4$ moves. The star illustrates the fact that the system can appear in different trends (decreasing, stationary, or increasing number of cells) when viewed from different scales. The thick line on the abscissa marks the number of successful moves represented in the preceding figure.

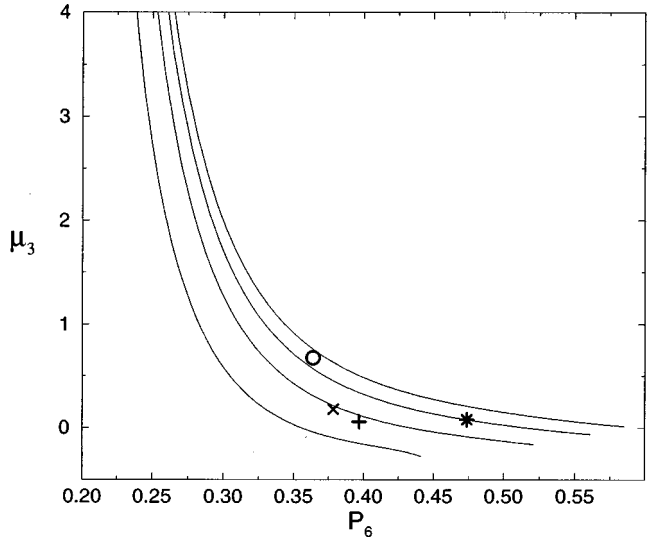


FIG. 10. The dynamic map $(p_6,\mu_3)$ of Fig. 3, enlarged, for the four families of division kernels, defined in the Appendix, with $g_i = 1$, 0.5, 0.13, and 0 from left to right. Points represent natural data. $*$, cucumber (0.474,0.08) [3]; $+$, human amnion (0.397,0.06) [3]; $\times$, cork (0.3784,0.1785); $\circ$, MDCK (statistics computed from pictures of MDCK cells, given by Wegener, and cultured as in [4]). Cells in the cork and human amnion divide similarly, less symmetrically than in cucumber epithelium. The cultured MDCK cells are highly disordered, yet divide almost perfectly symmetrically.

used to perform (time-consuming) topological simulations with the same characteristics as the biological tissues.

### B. The human epidermis

As shown in [5], 2D froths can be used to model realistically the renewal of mammalian epidermal tissues. Such tissues have a layered structure that can be regarded as a fluid of cells filling at random the space between the dermis and the outer surface (horny layer). The renewal of epidermal tissues depends on the dynamics of their innermost one-cell-deep layer—the basement layer—which is the only place where cells divide. The cells of the basement layer can either divide or detach to ascend in the upper layers. The set of attachments of these cells on the dermis is very similar to a 2D froth evolving with cell divisions and cell disappearances.

In [5], it was found that equations 1 admitted only one solution that fulfilled the steady-state constraint: $\Sigma_k p_k P_m(k) D_m(k) = \Sigma_k p_k P_d(k) D_d(k)$. This solution is associated to the parameters $P_m(k)D_m(k) = (5.11-k)^8$ and $P_d(k)D_d(k) = (7.01-k)^8$.

We simulated a tissue evolving with parameters reproducing those of the numerical solution. This system is mode *h* of Sec. IV. The distribution obtained is given in Table IV and is compared to the experimental data and the numerical solution. The concordance between the three distributions is very good.

The evolution of the simulated system is very sensitive to the values of $P(m|k)$ and $P(d|k)$ for $4 \leqslant k \leqslant 8$. For example, increasing $P(d|4)$ from 0.515 to 0.516 yields a system that dies away after $863 \times 10^5$ moves. The same result is obtained after $717 \times 10^5$ moves if $P(m|8)$ is changed from 0.500 to 0.499.

## VI. CONCLUSIONS

We have studied the evolution of epithelial tissues formed from confluent cells using 2D topological foams. Two types of tissues were analyzed: those evolving with cell divisions only, such as the cucumis epithelia, the cork, or the amnion, and those evolving with both cell divisions and cell disappearances, such as the basement membrane, the innermost layer of the human epidermis. The tissues were assimilated to a planar graph of cell edges and threefold vertices: a 2D topological froth.

The rate equation governing the variation of the number of *s*-sided cells of a froth evolving with divisions only has been solved numerically for a variety of division kernels and a wide range of $P_m(k)D_m(k)$, the conditional probability that a *k*-sided cell divides per unit of time. We classified the solutions in families containing systems with the same division kernel. Each solution is characterized by $\mu_3$ and $p_6$. For each family, we obtained a continuous curve $\mu_3(p_6)$. The curves for different families do not intersect. The relation $\mu_3(p_6)$ is therefore characteristic of the family. If one knows the third moment of a distribution $p_s$ and the probability that a six-sided cell exists, one can deduce the symmetry of the division kernel and the conditional probability per unit of time, $P_m(k)D_m(k)$, that a *k*-sided cell divides. From the stationary distribution, we can infer the dynamics of cell division. We used this technique to predict the symmetry of the division kernel and $P_m(k)D_m(k)$ for the epithelia of the cucumis, the cork, the human amnions, and the cultured MDCK. The predictions are in very good agreement with the data available for the cucumber [3].

We have performed topological simulations of systems evolving with divisions only and with divisions and detachments. When only divisions are performed, we showed that the systems evolve toward a steady state whatever initial froth is chosen. The convergence is very fast when the systems converge to a froth with a small $\mu_2$, but can be slower if $\mu_2$ is larger. We were able to produce steady-state froths with a very different amount of disorder from $\mu_2 < 0.45$ to $\mu_2 > 30$.

When both divisions and detachments are performed, the evolution of the system is a mixture of two competing

TABLE IV. Distributions obtained with the simulation compared to the experimental data and the numerical solution.

| $k$ | 3 | 4 | 5 | 6 | 7 | 8 | $\geqslant 9$ |
|---|---|---|---|---|---|---|---|
| $p_k$ (simulation) | 0 | 0.006 | 0.214 | 0.571 | 0.194 | 0.014 | 0 |
| $p_k$ (experiment) | 0 | 0.012 | 0.208 | 0.566 | 0.194 | 0.020 | 0 |
| $p_k$ (theory) | 0 | 0.002 | 0.218 | 0.564 | 0.199 | 0.007 | 0 |

mechanisms: gain of cells and loss of cells. We analyzed the evolution of systems in statistical equilibrium, for which, on average, the gain of cells compensates the loss of cells. When the systems are highly disordered, their second moment exhibits large fluctuations. When they have small $\mu_2$, the fluctuations are much smaller. In all cases, the distributions are stationary after some time and within statistical fluctuations. The temporal evolution of the systems over a long time is characterized by a scale-invariant evolution of their number of cells $N(t)$. Over a long time, $N(t)$ can increase or decrease by a factor of 5. We showed that the general evolution of systems evolving with division and detachment is independent of the initial disorder of the froth and of its size. The information contained in $P(m|k)$ and $P(d|k)$ and $\Gamma(k\rightarrow s)$ thus determines the eventual statistical state of the system.

We simulated the evolution of the innermost layer of the epidermis, the basement membrane. The distribution obtained by simulation is in very good agreement with experimental data and with the analytic solution.

The main conclusion of this work is that purely topological information limited to the cell suffices to explain the stability and the evolution of biological tissues evolving with division and/or detachment. No additional information (specific cell-cell correlation or long-range signal) is needed.

The approach we developed can be applied to all types of tissues made of confluent cells evolving through division and/or disappearance, regardless of the species considered. For such tissues, the predictions we made in Secs. III and V give qualitative information on the cell dynamics. Our predictions are exact when the functional forms of the parameters of division are known. These functional forms can be deduced directly or indirectly from experiments, as has been done in [2].

We have shown that purely topological information on an individual cell determines its fate, and suffices to explain the stability and evolution of biological tissues. Specifically, in the mammal's epidermis, basal cells whose 2D attachment on the basement membrane has five sides or fewer detach, while 2D cells with seven sides or more divide, as symmetrically as possible.

## APPENDIX

Here, we define the division kernels $\Gamma(k\rightarrow s)$ introduced in Sec. II and used to obtain Figs. 3 and 10.

One of the main parameters controlling the topological division of a cell is the symmetry with which it divides. For instance, a six-sided cell may divide symmetrically in two five-sided daughters, more asymmetrically into a six- and a four-sided daughter, or fully asymmetrically into a three- and a seven-sided cell.

In our model, the symmetry of the division is controlled by the kernel of division $\frac{1}{2}\Gamma(k\rightarrow s)$, introduced in Sec. II. It is the conditional probability that a daughter cell produced by the division of an existing dividing $k$-sided cell has $s$ sides. For symmetric $\Gamma$, we expect cellular systems whose dynamics include cellular division to evolve toward a steady-state characterized by narrower distributions and smaller $\mu_2$. Conversely, asymmetric $\Gamma$ are expected to yield more disorganized systems.

$\Gamma(k\rightarrow s)$ is constrained by three relations [2]:

$$\Gamma(k\rightarrow s)=\Gamma(k\rightarrow k+4-s), \tag{A1}$$

$$\sum_s \Gamma(k\rightarrow s)=2, \tag{A2}$$

$$\sum_s s\Gamma(k\rightarrow s)=k+4. \tag{A3}$$

If a $k$-sided cell divides into an $s$-sided daughter cell, it also produces a $(k+4-s)$-sided daughter [relation (A1)]. $\Gamma(k\rightarrow s)$ is normalized to 2 with relation (A2) [the division kernel $\frac{1}{2}\Gamma(k\rightarrow s)$ is normalized to 1]. Relation (A3) is a consequence of the symmetry of $\Gamma(k\rightarrow s)$. We studied five different types of division kernel ($\Gamma_i$, $i=1,\ldots,5$) associated with increasing degrees of symmetry as $i$ increases.

(i) $\Gamma_1$ is the most asymmetric kernel. Each dividing $k$-sided cell produces a three- and a $(k+1)$-sided daughter. This kernel yields the most disordered structures (highest $\mu_2$), similar to the fractal patterns that one obtains by systematic vertex decoration with a three-sided cell [12].

(ii) $\Gamma_2$ is a broad, flat kernel. $\Gamma_2(k\rightarrow s)=2/(k-1)$ $(3\leqslant s\leqslant k+1)$. A $k$-sided cell is fragmented into two cells by an edge which bisects two different sides chosen at random among its $k$ sides. (The two sides must be different to avoid two-sided cells.)

(iii) For $\Gamma_{i\geqslant 3}$, we used the following functional form, parametrized with the number $g_i$: $g_3=1$, $g_4=0.5$, $g_5=0$.

For $3\leqslant k\leqslant 8$,

| $k/s$ | 3 | 4 | 5 | 6 | 7 | 8 | $>8$ |
|---|---|---|---|---|---|---|---|
| 3 | 1 | 1 | 0 | 0 | 0 | 0 | 0 |
| 4 | $g_i$ | $2-2g_i$ | $g_i$ | 0 | 0 | 0 | 0 |
| 5 | $g_i/4$ | $1-g_i/4$ | $1-g_i/4$ | $g_i/4$ | 0 | 0 | 0 |
| 6 | $g_i/8$ | $3g_i/8$ | $2-g_i$ | $3g_i/8$ | $g_i/8$ | 0 | 0 |
| 7 | 0 | $g_i/4$ | $1-g_i/4$ | $1-g_i/4$ | $g_i/4$ | 0 | 0 |
| 8 | 0 | $g_i/8$ | $3g_i/8$ | $2-g_i$ | $3g_i/8$ | $g_i/8$ | 0 |

For $k \geqslant 9$, if $k$ is even,

$$\Gamma_i[k \to (k+4)/2] = 2 - g_i,$$

$$\Gamma_i[k \to (k+4)/2-1] = \Gamma_i[k \to (k+4)/2+1] = \frac{g_i}{3},$$

$$\Gamma_i[k \to (k+4)/2-2] = \Gamma_i[k \to (k+4)/2+2] = \frac{g_i}{9},$$

$$\Gamma_i[k \to (k+4)/2-3] = \Gamma_i[k \to (k+4)/2+3] = \frac{g_i}{18}.$$

If $k \geqslant 9$ is odd,

$$\Gamma_i[k \to (k+1)/2+2] = \Gamma_i[k \to (k-1)/2+2] = 1 - \frac{g_i}{4},$$

$$\Gamma_i[k \to (k+1)/2+3] = \Gamma_i[k \to (k-1)/2+1] = \frac{3g_i}{6},$$

$$\Gamma_i[k \to (k+1)/2+4] = \Gamma_i[k \to (k-1)/2] = \frac{g_i}{6},$$

$\Gamma_i = 0$ otherwise.

$\Gamma_5$ is the most symmetric kernel. A $(k=2n)$-sided cell divides into two $(n+2)$-sided cells and a $(k=2n+1)$-sided cell divides into daughter cells with $n+3$ and $n+2$ sides. It corresponds to the rightmost curve of Fig. 3. $\Gamma_4$ is slightly asymmetric. $\Gamma_3$, more asymmetric than $\Gamma_4$, is qualitatively halfway between $\Gamma_2$ and $\Gamma_5$.


[1] L. J. Gibson and M. Ashby, *Cellular Solids* (Pergamon, New York, 1988).

[2] N. Rivier, X. Arcenegui Siemens, and G. Schliecker, *Cell Division and Evolution of Biological Tissues*, in *Fragmentation Phenomena*, edited by D. Beysens, X. Campi, and E. Pefferkorn (World Scientific, Singapore, 1995), pp. 267–282.

[3] F. T. Lewis, Anat. Rec. **38**, 341 (1928).

[4] A. Janshoff, J. Wegener, M. Sieber, and H.-J. Galla, Eur. Biophys. J. **25**, 93 (1996).

[5] B. Dubertret and N. Rivier, Biophys. J. **73**, 38 (1997).

[6] N. Rivier, in *Disorder and Granular Media*, edited by D. Bideau and A. Hansen (North Holland, Amsterdam, 1993), pp. 55–102.

[7] R. Delannay and G. Le Caër, Phys. Rev. Lett. **73**, 1553 (1994).

[8] M. A. Peshkin, K. J. Strandburg, and N. Rivier, Phys. Rev. Lett. **67**, 1803 (1991).

[9] B. Dubertret, N. Rivier, and M. A. Peshkin, J. Phys. A **31**, 879 (1998).

[10] N. Rivier, in *From Statistical Physics to Statistical Inference and Back*, edited by P. Grassberger and J.-P. Nadal (Kluwer, Dordrecht, 1994), pp. 77–93.

[11] J. Lemaitre, A. Gervois, J.-P. Troadec, N. Rivier, M. Ammi, L. Oger, and D. Bideau, Philos. Mag. B **67**, 347 (1993).

[12] G. Le Caër and R. Delannay, J. Phys. I **5**, 1417 (1995).